JOURNAL OF CATALYSIS 148, 224–239 (1994)

A Transient Kinetic Study of the CO/H_2 Reaction on Rh/Al_2O_3 Using FTIR and Mass Spectroscopy

A. M. Efstathiou,*[,1] T. Chafik,† D. Bianchi,† and C. O. Bennett*

*Department of Chemical Engineering, University of Connecticut, Storrs, Connecticut 06269-3139; and †Laboratoire des Materiaux et Procedes Catalytiques, Universite Claude Bernard Lyon I, 43 Boulevard du 11 Novembre 1918, Villeurbanne 69622, Villeurbanne Cedex, France

Received November 29, 1993; revised February 11, 1994

The evolution of surface species (their chemical composition and surface coverage) formed during the CO/H_2 reaction at 220°C on 1 wt% Rh/Al_2O_3 catalyst was studied by transient isotopic and various hydrogen titration techniques using both *in situ* mass spectrometry and FTIR. There is a very small amount of active carbon, CH_x ($\theta_{CH_x} < 0.03$), and a large amount of surface linear and bridged CO species ($\theta_{CO} = 0.93$) which participate in the formation of CH_4 during reaction. Their amounts stay practically constant with reaction time in CO/H_2 even after 1 h on stream. Also present on the Rh surface are some C_xH_y (alkyl chains) species which largely grow with reaction time (during the first hour on stream) but do not participate in the reaction mechanism of CH_4 formation (spectator species). In addition, formate and carbonate (spectator species) build slowly on the alumina support surface even after 1 h of reaction. The surface coverage of hydrogen, θ_H, is found to be very small, a result consistent with the coverages of CO, CH_x, and C_xH_y species. CO dissociation over the present 1 wt% Rh/Al_2O_3 (1.5-nm Rh particles) appears to largely control the overall rate of methane formation, a result similar to that previously reported over the 5 wt% Rh/Al_2O_3 (9.0-nm Rh particles) catalyst.

INTRODUCTION

Knowledge of the state of a catalyst surface during reaction is an ultimate goal in order to understand catalytic reactions. In particular, determination of the surface coverage of intermediate species in a reaction network and the intrinsic rate constant, k, of individual reaction steps, which is proportional to the reactivity of a given intermediate species, has long been appreciated as an important aim of fundamental research in heterogeneous catalysis. First Happel *et al.* (1, 2) and later Biloen and co-workers (3–5) introduced the use of steady-state tracing techniques for the determination of the intrinsic rate constant, k, and the fractional surface coverage, θ, of reaction intermediates for the CO/H_2 reaction. These techniques have been successfully applied by other investigators later to study the mechanism of the CO/H_2 reaction over group VIII metal-supported catalysts (6–17), ammonia synthesis (18), and, recently, oxidative coupling of methane to C_2-hydrocarbons (19–21).

Most of the transient work in CO/H_2 reaction has in the past been conducted using a mass spectrometer as a detector, permitting an accurate quantitative insight into the dynamics of the surface reaction processes that occurred. On the other hand, it is sometimes difficult to know the exact nature of adsorbed intermediate species using only mass spectrometry. Transient FTIR spectroscopy is another powerful tool to study the dynamics of a surface reaction network and identify surface adsorbed intermediate species formed during reaction conditions (22). Combining transient FTIR and mass spectroscopies has the advantages of correctly characterizing a given surface reaction intermediate species (its chemical composition and surface coverage) (23, 24), and distinguishing between adsorbed reaction intermediate and spectator species (25), as the present work also illustrates.

The focus of this work is to apply the steady-state tracing and other transient techniques using both mass and FTIR spectroscopies to study the working surface state of 1.5-nm Rh particles supported on Al_2O_3 for the CO/H_2 reaction at 220°C and 1 bar. The present results are compared to those reported for 9.0-nm Rh particles supported on Al_2O_3 under the same reaction conditions (6, 7).

EXPERIMENTAL

(1) Catalyst Preparation

A 0.95 wt% Rh/γ-Al_2O_3 catalyst was prepared by impregnating Alon-C (Degussa) to incipient wetness with an aqueous solution of $RhCl_3 \cdot 3H_2O$ (Aldrich Chemical Co.). The powder was dried at room temperature for 96 h followed by 2 h drying at 105°C, pressed at 2000 psi, crushed, and then sieved to give 0.58- to 0.84-mm particles. For

[1] Present address: Institute of Chemical Engineering and High Temperature Chemical Processes, GR-26500, Patras, Greece.

0021-9517/94 $6.00

storage it was passivated by treatment in H_2 at 300°C for 2 h followed by treatment in O_2 at 400°C for 2 h.

Before any transient experiments with mass spectrometry were performed, the fresh charged catalyst (45 mg) was reduced in H_2 at 350°C for 2 h, and then treated with H_2/CO mixture for 2 h at 220°C to obtain a fairly stabilized surface for subsequent experiments. After a given run, the temperature was raised to 450°C under H_2 and held for 15 min until no methane was detectable. Then the catalyst was brought to reaction temperature under H_2 flow.

Transient FTIR experiments were performed on a fresh catalyst sample (45 mg) which was pressed into a self-supporting disk of about 0.1 mm thickness and 21 mm diameter and placed in the IR reactor cell of 1 mL internal volume.

(2) *Catalyst Characterization*

The BET surface area of the alumina (110 ± 5 m^2/g) was measured in a flow sorption apparatus described elsewhere (26). The active metal surface area was obtained by extrapolating the linear part of the H_2 chemisorption isotherm at 298 K to zero pressure and assuming $H/Rh_S = 1.0$ (27). The hydrogen uptake of the catalyst was found to be 32.5 μmol H_2/g cat, yielding a value of 65 μmol Rh surface atoms/g of catalyst. The fraction exposed, *FE*, of the Rh was found to be 0.65. Assuming spherical particles and an average Rh atom area of 7.9×10^{-20} m^2 yielded an average particle size of 1.5 nm. H_2 chemisorption at room temperature from a 5% H_2/Ar mixture, followed by temperature-programmed desorption (TPD) with mass spectrometer as a detector, yielded the amount of chemisorption obtained from the isotherm, within 10%, as mentioned above. In addition, the same H_2 chemisorption/TPD experiment performed at the end of all the transient experiments presented in this work provided the same uptake, within 5%, as that measured on the fresh catalyst sample (before exposure to the CO/H_2 mixture).

(3) *Reactor and Flow System*

A once-through stainless steel microreactor of 0.5 mL internal volume was used for transient studies with mass spectrometry. The behaviour of the reactor was that of a true CSTR as previously reported (9, 10). The integrity of the transient results, free of any flow disturbances by switching the valves, was maintained as described elsewhere (28, 29). The stainless steel FTIR cell of 1 mL internal volume used under transient conditions was of specific design, details of which were given elsewhere (30). FTIR spectra can be recorded at the reaction temperature between 25 and 600°C under a flow of gas varying in the range of 150–300 cm^3/min (ambient conditions). The latter values of the flow rate are appropriate to ensuring a fast response in the change of the feed gas composition which the catalyst surface experiences.

The H_2/CO and He/CO gas mixtures were prepared based on 9.9 mol% CO, while for the H_2/CO mixture the appropriate H_2 composition was used to give a ratio of $H_2/CO = 9$ with He as a balance. Preparation of $H_2/{}^{13}CO = 9$ mixture has been described in detail elsewhere (7). One percent Ar was also added to the $H_2/{}^{13}CO$ mixture to facilitate obtaining the forcing (F) and mixing (M) curves (10) needed to interpret the steady-state tracing experiments. The $He/{}^{13}CO$ mixture had 99.3% ^{13}C.

The flow rate of all gases used during transient experiments with mass spectrometry was 30 mL/min (ambient). At this flow rate the mean residence time in the reactor was 1 s. The He and Ar gases used were UHP and the H_2 standard (99.98%). Further purification of these gases was performed as previously described (9, 10).

(4) *Mass and FTIR Spectrometry*

Calibration and data acquisition of the high resolution mass spectrometer (Nuclide 12-90-G) responses obtained have been described in detail elsewhere (6, 31). Mass numbers used were 2, 15, 17, 28, 29, 40, and 44 for H_2, CH_4, $^{13}CH_4$, CO, ^{13}CO, Ar, and CO_2, respectively. The FTIR spectrometer (Nicolet, model 5DX-C) had the capability of recording one spectrum (averaged)/sec using the SX software of the data acquisition system provided.

RESULTS

The surface composition of the 1 wt% Rh/Al_2O_3 catalyst under CO/H_2 reaction conditions at 220°C has been determined using both transient mass spectrometry and FTIR. For this, steady-state tracing (use of ^{13}CO), transient hydrogenation of carbonaceous intermediate species, and H_2 chemisorption, following CO/H_2 reaction, experiments have been performed. The experiments conducted using mass spectrometry are first described, followed by those using FTIR. ^{13}CO/He exchange experiments performed after reaction in CO/H_2, followed by TPD, are also presented to facilitate the interpretation of some of the transient results obtained under CO/H_2 reaction conditions.

(1) *Transient Mass Spectrometry*

(1a) Steady-state tracing. Figure 1 shows the response of the reactor outlet composition after the switch $^{12}CO/H_2/He$ (120s) → $^{13}CO/H_2/He/Ar$ (t) at 220°C is made. The results are expressed in terms of the variable Z, which represents the fraction of the ultimate change (giving $Z = 1$) as a function of time. Thus, Z is defined by

$$Z(t) = (y(t) - y_0)/(y_\infty - y_0), \qquad [1]$$

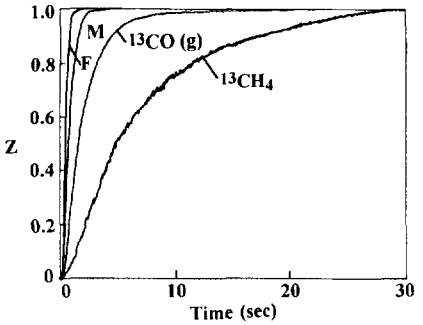

FIG. 1. Dimensionless experimental responses of forcing (F), mixing (M), gas-phase ^{13}CO, and $^{13}CH_4$ obtained according to the delivery sequence $^{12}CO/H_2/He$ (120 s) → $^{13}CO/H_2/He/Ar$ (t). T = 220°C, H_2/CO = 9, P_{CO} = 0.1 bar, and X_{CO} = 0.6%.

where the subscripts 0 and ∞ refer to values of y (mole fraction) just before the switch ($t = 0$) and long after the switch ($t \to \infty$). The curve F (forcing) is obtained from the argon response ($y_0 = 0$, $y_\infty = 0.01$) as the gas flows through a bypass around the reactor (9). The curve M (mixing) is the response of the argon as this passes through the reactor containing the catalyst. As already discussed elsewhere (10, 31), curve M can be represented by the response of a mixed-flow reactor (CSTR) to the forcing function F. For the curve labeled $^{13}CO(g)$, y represents the fraction of ^{13}CO in the gaseous CO at the reactor outlet. Thus, if there were no adsorption or reaction of CO, $^{13}CO(g)$ and M curves would be identical. It can be shown by a material balance that the area difference between the actual $^{13}CO(g)$ response shown in Fig. 1 and that of the mixing curve (M) is proportional to the amount of CO adsorbed under reaction conditions, assuming that all the surface ^{12}CO is replaced by ^{13}CO (31). Based on this, it is calculated that the surface coverage of CO is 0.95. Further experiments at 220°C for times in $^{12}CO/H_2$ between 30 and 3600 s give values of θ_{CO} in the range of 0.95–0.92. Thus, the surface coverage of CO remains practically constant even after 1 h of reaction.

The correct interpretation of the observed $^{13}CH_4$ response in Fig. 1 requires the following to be stated. It is assumed that the reaction sequence passes from adsorbed CO irreversibly to an adsorbed intermediate carbon species, CH_x, which is irreversibly and sequentially hydrogenated to CH_4. Thus, the dynamics of the appearance of $^{13}CH_4$ is related to the rate of change of adsorbed ^{12}CO to ^{13}CO and to the amount of intermediate species after the adsorbed CO for which the carbon content must change from ^{12}C to ^{13}C. The analytical equations representing these processes have been developed and applied as indicated elsewhere (7–11, 31). The experimental Z for the $^{13}CH_4$ response can be modeled, and a τ_{CH_x} (mean life time) value of the CH_x intermediate species, from which CH_4 is eventually produced, can be calculated (10, 31). Then the coverage of these intermediate species, θ_{CH_x}, is obtained via

$$\theta_{CH_x} = TOF_{CH_x} \cdot \tau_{CH_x}, \qquad [2]$$

where TOF_{CH_x} is the turnover frequency for the total production of hydrocarbons for the conditions at hand ($TOF_{CH_x} = 4.0 \times 10^{-3}\ s^{-1}$). Values of τ_{CH_x} between 3.5 and 4.5 s are found to best describe the $^{13}CH_4$ response shown in Fig. 1. Thus, θ_{CH_x} is estimated to be in the range of 0.015–0.018 of a monolayer. The CO conversion and the CH_4 selectivity obtained are found to be 0.6 and 95%, respectively.

(1b) Transient isothermal hydrogenation followed by TPR of the adsorbed carbon-containing species formed after CO/H_2 reaction at 220°C. In the isothermal experiment of Fig. 2a there is an initial transient (peak 1) as the reaction in CO/H_2 starts from a practically clean surface (after H_2 reduction and He purge at 350°C), followed by

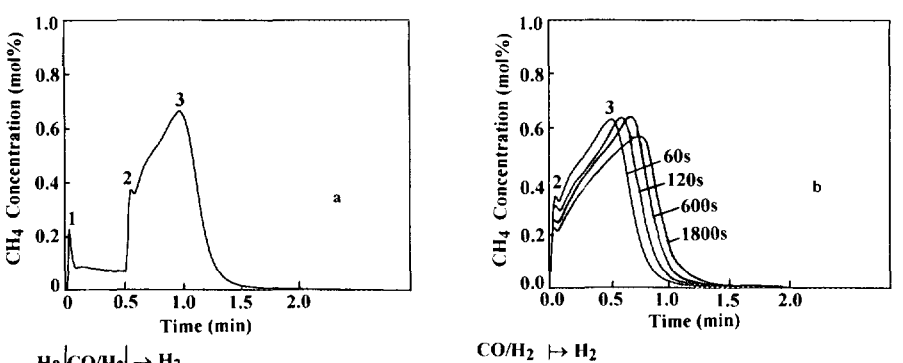

FIG. 2. (a) Transient response of CH_4 at 220°C according to the delivery sequence He (180 s) → H_2/CO (30 s) → H_2 (t). The numbering system for identifying the peaks is shown. Peak 1: that obtained at the start of reaction, He → H_2/CO; peak 2: first spike obtained after reaction for 30 s, caused by the switch $CO/H_2 \to H_2$; peak 3: broad peak obtained after peak 2, caused by hydrogenation at 220°C of adsorbed carbon-containing species formed after 30 s in H_2/CO. (b) Transient responses of CH_4 at 220°C obtained under H_2 switch according to the delivery sequence He (180 s) → H_2/CO (Δt) → H_2 (t). Δt = 60, 120, 600, and 1800 s.

a period of pseudo-steady-state under CO/H_2. Titration of the adsorbed carbon-containing species formed under reaction conditions with H_2 leads to a second CH_4 transient which produces peaks 2 and 3. Much information is contained in the peak heights and shapes, and in the areas under these curves. These and other transient results described below are used to estimate the composition of the working surface of Rh/Al_2O_3 catalyst and to extract kinetic parameters of the hydrogenation process of the adsorbed carbon species.

The first sharp peak (peak 1) in Fig. 2a occurs as H_2/CO starts to flow over the catalyst, and it is expected to grow with temperature as observed over a previous study on 5 wt% Rh/Al_2O_3 catalyst (6). A switch to H_2 after 30 s of reaction produces both the sharp peak 2 and the broad peak 3 of CH_4 with a shoulder between them. At 220°C, the rate of hydrogenation falls to zero within about 2 min. Of interest was to study this hydrogenation process as a function of time on stream, Δt, in H_2/CO.

Figure 2b shows transient hydrogenation results of CH_4 production at 220°C after 60, 120, 600, and 1800 s of H_2/CO reaction. Various features observed in the CH_4 transients of Fig. 2b should be noted. The height of the sharp peak 2 diminishes with increasing time on stream, whereas peak 3 grows with time on stream and it takes longer to reach its maximum, t_m, under H_2 flow. The latter behaviour is further studied by using ^{13}CO isotope gas and a kinetic model developed as described below. Integration of the CH_4 transients of Fig. 2b provides the amounts of carbonaceous species hydrogenated to CH_4 at 220°C. Table 1 summarizes the quantitative aspects of the transient isothermal hydrogenation kinetics shown in Figs. 2a and 2b. Column 3 in Table 1 gives the amount (monolayers) of carbonaceous species hydrogenated isothermally at 220°C, whereas column 2 gives the time, t_m, of appearance of the maximum of peak 3 under H_2 reaction at 220°C. Note that in column 3 the coverage of the adsorbed carbonaceous species increases with time on stream and is higher than one (assuming one carbon atom per surface Rh atom), a result which indicates that some of the adsorbed species contain more than one carbon atom. These issues are discussed below with respect to the transient FTIR results obtained for the same experiment.

TABLE 1

Coverage of Surface Carbon-Containing Species Hydrogenated to CH_4, and Time of Appearance of Peak 3 Maximum, t_m, According to the Sequence CO/H_2(220°C, Δt) → H_2(220°C, t) → TPR

Time in CO/H_2 (Δt) (s)	t_m (s)	220°C (monolayers)	TPR (monolayers)	Total (monolayers)
30	26	1.52	—[a]	1.52
60	32	1.62	—[a]	1.62
120	36	1.69	0.05	1.74
600	42	1.84	0.21	2.05
1800	47	1.88	0.49	2.37
3600	51	1.86	0.84	2.70

[a] Not present.

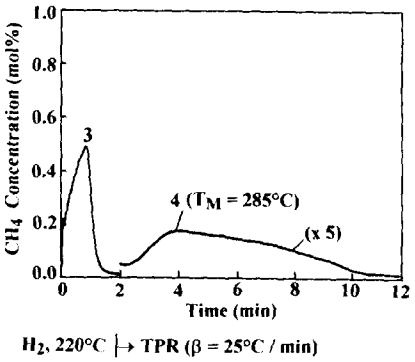

FIG. 3. Transient response of CH_4 according to the delivery sequence He (180 s) → H_2/CO (220°C, 1 h) → H_2 (220°C, 120 s) → TPR (β = 25°C/min). Peak 4 is obtained during H_2 TPR after the completion of isothermal hydrogenation.

Temperature-programmed reaction (TPR) experiments in H_2 flow, following the isothermal experiments of Fig. 2, reveal that for times in CO/H_2 reaction greater than about 120 s, less active carbonaceous species accumulate on the surface. Figure 3 presents such an experiment after 1 h of reaction in CO/H_2 at 220°C. Peaks 2 (spike) and 3 appear under the isothermal hydrogenation at 220°C, as in Fig. 2, while after 2 min in H_2 flow the temperature is increased to 450°C (β = 25°C/min). A broad peak 4 is then produced with a peak maximum at T_M = 285°C and a tail out to 450°C. The amounts of less active carbonaceous species, not hydrogenated to CH_4 at 220°C, as a function of time on stream, Δt, are given in Table 1, column 4. The total amount of carbon-containing adsorbed species measured based on the CH_4 response (isothermal + TPR) is given in column 5.

(1c) Transient isotopic deconvolution experiment of the CH_4 response. Figure 4a shows an isotopic deconvolution of the CH_4 transient isothermal hydrogenation responses presented in Fig. 2. The experiment was as follows. After reaction in CO/H_2 for time Δt, the reaction is quenched by a switch from $^{12}CO/H_2$ to ^{13}CO/He for 30 s, before an isothermal hydrogen titration is performed. During the exposure to ^{13}CO/He (30 s), methane production stops, while the $^{12}CH_x$ is not replaced by new $^{13}CH_x$. However, adsorbed ^{12}CO exchanges rapidly with gaseous ^{13}CO, as already shown in Fig. 1. Thus, in Fig. 4a the $^{13}CH_4$ peaks arise from adsorbed ^{13}CO, and the $^{12}CH_4$ peaks (peaks 2 and 3) arise from carbonaceous adsorbed species which do not exchange with gaseous or adsorbed ^{13}CO. A very small amount of new elementary ^{13}C may

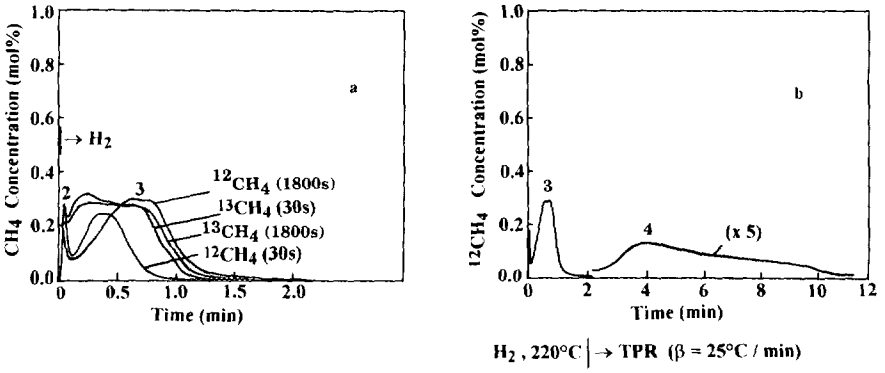

FIG. 4. (a) Transient isotopic experiment for deconvoluting the CH_4 response obtained in Fig. 2 according to the delivery sequence He (180 s) → CO/H_2 (Δt) → ^{13}CO/He (30 s) → H_2 (t). T = 220°C, Δt = 30 s and 1800 s. (b) Transient response of $^{12}CH_4$ obtained according to the delivery sequence described in (a) for Δt = 1800 s. After the isothermal hydrogenation at 220°C for 120 s, a TPR (β = 25°C/min) process is performed.

be produced by ^{13}CO disproportionation and may contribute to the initial $^{13}CH_4$ peak.

Taking into account the comments mentioned in the previous paragraph, and comparing the transient isothermal hydrogenation results of Figs. 2b and 4a after 30 s in CO/H_2, it appears that the sharp initial peak of $^{12}CH_4$ response in Fig. 4a is due to the $^{12}CH_x$ species, which is easily hydrogenated, while the second broad peak is due to less active species identified as alkyl chain C_xH_y species (using transient FTIR). The $^{13}CH_4$ response gives a small but sharp initial peak (due to elementary ^{13}C carbon formed during the 30 s of ^{13}CO/He treatment) and a second broad peak due to the hydrogenation of exchangeable surface CO species. For longer times on stream (1800 s), the same feature is obtained but now the $^{13}CH_4$ response is almost the same as that obtained after 30 s on stream in CO/H_2, while the $^{12}CH_4$ response is different. In particular, the $^{12}CH_4$ peak 3 increases and its maximum shifts to a higher t_m value. Note also that the height of the initial $^{12}CH_4$ peak 2 decreases but, practically, without a shift of its maximum. Table 2 gives the quantity of $^{12}CH_4$ (column 2) and $^{13}CH_4$ (column 3) production as well as the total amount of equivalent carbon (column 4) as a function of time on stream in CO/H_2. A good agreement between column 4 in Table 2 and column 3 in Table 1 is obtained.

The deconvolution experiment shown in Fig. 4a allows one to interpret correctly the CH_4 responses of Fig. 2b. Peak 2 in Figs. 2a and 2b is due to the hydrogenation of a very active CH_x species (not exchangeable with ^{13}CO). Peak 3, which is observed in Figs. 2a and 2b, arises from the hydrogenation of two kinds of adsorbed carbon species. One is the surface CO, which readily exchanges with gaseous ^{13}CO, and the other one is the C_xH_y species which does not exchange with ^{13}CO. The hydrogenation of these two species produces peak 3, an initial shoulder followed by a distinct maximum. The growing and shifting of this maximum with time on stream is caused by the growth of the C_xH_y species because the $^{13}CH_4$ response due to adsorbed CO species stays constant with time on stream (Fig. 4a). The shoulder seems to be due to the hydrogenation of CO adsorbed species.

A TPR experiment in H_2 flow, following that of isothermal hydrogenation after 1800 s of reaction in CO/H_2 (Fig. 4a), reveals that less active carbonaceous species which do not exchange with ^{13}CO at 220°C accumulate on the catalyst surface (Fig. 4b); note that no $^{13}CH_4$ is detected during this H_2 TPR. The amount of the less active nonexchangeable carbonaceous species is given in Table 2, column 2 as a function of time in CO/H_2 reaction. These results show that these species accumulate slowly on the catalyst surface.

(1d) Measurement of hydrogen coverage during CO/H_2 reaction at 220°C. The total quantity of carbonaceous adsorbed species formed on the rhodium surface exceeds the monolayer value (see Table 1, column 5). This means that during CO/H_2 reaction the number of sites for hydrogen chemisorption must be very low. Attempts were made to measure this surface hydrogen coverage. After reaction

TABLE 2

Coverage of Surface Carbon-Containing Species Hydrogenated to CH_4 According to the Delivery Sequence CO/H_2 (220°C, Δt) → ^{13}CO/He (30 s) → H_2 (t), TPR

Time in CO/H_2 (Δt) (s)	$^{12}CH_4$ (monolayers)	$^{13}CH_4$ (monolayers)	Total (monolayers)
30	0.54	0.97	1.51
600	0.90 (1.05)[a]	0.96	1.86 (2.01)
1800	0.96 (1.54)	0.95	1.91 (2.49)

[a] Number in parentheses includes less active carbonaceous species hydrogenated at $T > 220$°C.

in CO/H_2 for a period of time, t, the feed is changed to Ar for 30 s and the reactor is quickly cooled to 40°C followed by H_2 chemisorption (1 atm H_2, 10 min). The reactor is then purged with Ar for 120 s, while the temperature is increased to carry out a H_2 TPD. Two peaks of H_2 are observed: a first sharp peak at T_m around 100°C, followed by a broad peak at 350°C. Only the first peak is due to hydrogen chemisorption on the Rh surface (assignment based on the results obtained on a clean Rh/Al_2O_3 catalyst). The second peak is due to other adsorbed species, as is shown and discussed below. The first peak leads to a very low value for hydrogen coverage: θ_H = 0.05 and 0.02 for 30 s and 1/2 h on stream in CO/H_2, respectively, in agreement with the measured coverages of the other adsorbed carbonaceous species. These values indicate that a decrease of hydrogen sites occurs during CO/H_2 reaction. Note that these coverages represent an upper limit of the true surface coverage of hydrogen obtained during reaction since some CO may desorb during the cooling procedure applied before H_2 chemisorption. However, a small amount of adsorbed H_2 may react with the active CH_x species during TPD in the range 100–160°C (6, 7).

(2) *Transient FTIR Analysis of Adsorbed Species*

(2a) Adsorbed species formed during CO/H_2 reaction at 220°C. The population of adsorbed intermediate species on the surface of the 1 wt% Rh/Al_2O_3 catalyst during CO/H_2 reaction at 220°C was studied by *in situ* FTIR. Figures 5A and 5B show IR bands in the range 1150–2250 cm^{-1} and 2700–3100 cm^{-1}, respectively, for times on stream between 40 s and 1 h. The fresh catalyst sample, before reaction, was reduced in H_2 at 350°C for 1 h and purged in He for 10 min. After 40 s in CO/H_2, the IR bands recorded at 2046 and 1837 cm^{-1} (Fig. 5A, spectrum (a)) correspond to linear CO and bridged CO species, respectively. For times on stream in CO/H_2 larger than 160 s, the IR bands recorded at 1592, 1392, and 1378 cm^{-1} (Fig. 5A, spectra (c)–(e)) correspond to formate, COOH species, and the IR band at 1460 cm^{-1} to ionic carbonate adsorbed species. Figure 5B shows CH bands in the range 2700–3100 cm^{-1}. The bands recorded at 2950 and 2847 cm^{-1} with a shoulder at 2910 cm^{-1} (spectrum (d)) develop with increasing time on stream. These IR bands may not be attributed only to the formate species, which leads usually to two main IR bands in the range 3000–2800 cm^{-1} (around 2850 and 2950 cm^{-1}) with the intensity of the 2850 cm^{-1} band higher than that of the 2950 cm^{-1} band. Thus, other hydrocarbon species such as C_xH_y (alkyl chains) are present on the catalyst surface. The assignment of these IR bands is discussed below in some detail.

In Fig. 5A it is clearly observed that between 40 s and 1 h on stream the intensity of the linear CO species (IR bands at 2046 cm^{-1}) stays constant. However, the intensity of the bridged CO species increases slowly between 160 s and 30 min on stream, while it stays practically constant after 30 min of reaction. On the other hand, the coverage of both formate and carbonate adsorbed species still increases between 40 s and 1 h on stream; an increase by almost a factor of two can be seen between 1/2 h and 1 h on stream (spectra (d) and (e)). A similar behaviour is also obtained in Fig. 5B for the CH bands (C_xH_y and COOH species), where a continuous growth of these bands in the range of 40 s to 1 h on stream is noted. However, the increase in the intensity of the CH bands between 600 s and 1 h on stream (Fig. 5B spectra (c) and (d), respectively) is smaller than that observed in the case of COOH and CO_3^{2-} species.

(2b) Hydrogenation of adsorbed carbon-containing species formed after 1 h of reaction in CO/H_2 at 220°C. FTIR spectra recorded during isothermal hydrogenation (220°C) of adsorbed carbonaceous species

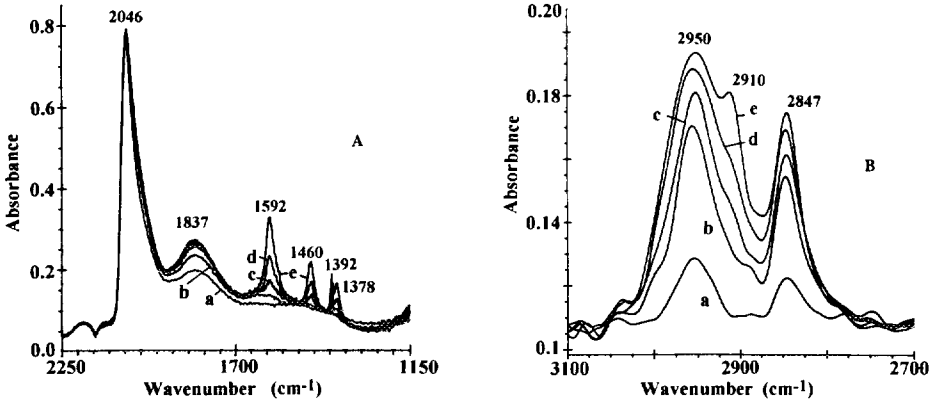

FIG. 5. (A) Transient FTIR spectra in the range of 1150–2250 cm^{-1} recorded at 220°C as a function of time on stream, t, in CO/H_2 over a reduced 1 wt% Rh/Al_2O_3 surface. (a) t = 40 s; (b) t = 160 s; (c) t = 600 s; (d) t = 1800 s; (e) t = 3600 s. (B) Transient FTIR spectra in the range of 2700–3100 cm^{-1} recorded at 220°C as a function of time on stream, t, in CO/H_2. (a)–(e) Same as in (A).

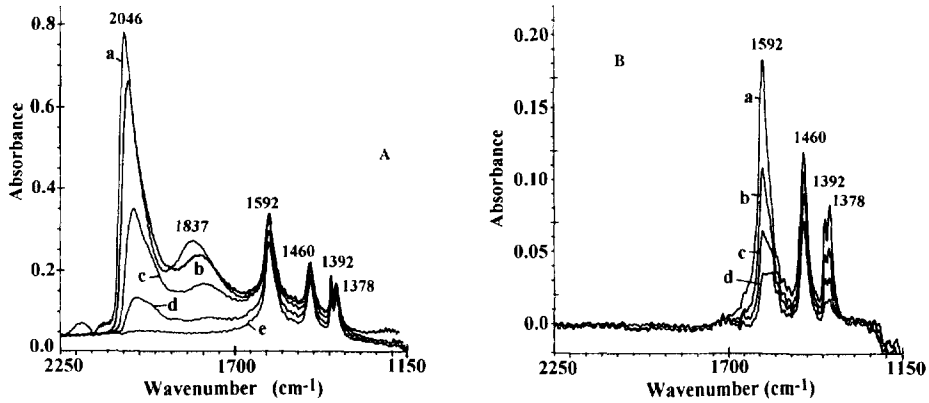

FIG. 6. (A) Transient FTIR spectra in the range of 1150–2250 cm^{-1} recorded at 220°C as a function of time on stream, t, in H_2 after CO/H_2 reaction at 220°C for 1 h. (a) t = 0 s; (b) t = 80 s; (c) t = 160 s; (d) t = 240 s; (e) t = 320 s. (B) FTIR spectra in the range of 1150–2250 cm^{-1} recorded during H_2 TPR, following CO/H_2 reaction at 220°C for 1 h and 320 s of isothermal hydrogenation at 220°C (see (A)). (a) T = 265°C; (b) T = 330°C; (c) T = 350°C; (d) T = 370°C.

formed after 1 h of reaction in CO/H_2 at 220°C are presented in Fig. 6A. During the first 4 min in H_2, almost all the linear and bridged CO species disappear. In contrast, there is only a small decrease in the surface coverage of COOH and CO_3^{2-} species after 320 s in H_2. Thus, these species do not significantly contribute to the CH_4 production presented in Figs. 2a and 2b. Formate and carbonate species disappear during H_2 TPR between 265 and 370°C (spectra (d) and (e), Fig. 6B).

Figure 7 shows the changes observed in the CH infrared bands (IR bands at 2950, 2910, and 2847 cm^{-1}) during hydrogenation at 220°C and also during a TPR process. Comparing spectra (a)–(c) it can be clearly seen that, after 3 min of hydrogenation reaction at 220°C, most of the CH infrared bands disappear, and part of the C_xH_y adsorbed species is hydrogenated at 220°C. The remaining IR bands, after 320 s in H_2 at 220°C, disappear during the TPR process (spectra (d) and (e)) and may be associated in part to formate species.

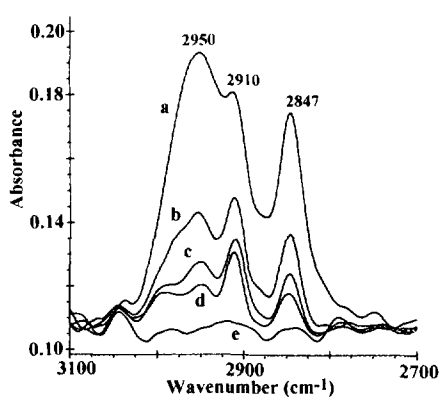

FIG. 7. FTIR spectra in the range of 2700–3100 cm^{-1} recorded during hydrogenation (isothermal at 220°C and TPR), following CO/H_2 reaction at 220°C for 1 h. (a) 220°C, t = 0; (b) 220°C, t = 120 s; (c) 220°C, t = 320 s; (d) T = 265°C; (e) T = 370°C.

(3) *Further Characterization of the Adsorbed Carbonaceous Species*

(3a) Kinetics of isothermal hydrogenation of C_xH_y adsorbed species at 220°C. It has been shown through the isotopic deconvolution experiment shown in Fig. 4a that peak 3, shown in Fig. 2b, is due to an overlap between two species, that of surface CO and C_xH_y. The isothermal deconvolution experiment showed also that it is the hydrogenation of the C_xH_y species which determines the time of appearance, t_m, of the maximum of peak 3. Thus, the shift of this peak (higher value of t_m) with time on stream in CO/H_2 (Fig. 2b) must be related to this species. A kinetic model developed by Bianchi and Gass (32) is used in the present work to study the isothermal hydrogenation of the C_xH_y species using the values of t_m observed.

A brief description of the model is appropriate. The assumed mechanism of hydrogenation of an adsorbed carbon-containing species to CH_4 is that of a stepwise addition of adsorbed hydrogen atoms (H*). If it is considered that there are α steps with the same rate constant k ($k = A \exp(-E_r/RT)$ which influence the rate of methane production (all other steps have rate constants $\gg k$), and the concentration of sites which chemisorb hydrogen, H, is constant during the hydrogenation process (a change by poisoning during CO/H_2 reaction might also be considered), then the following Eq. [3] is obtained (32):

$$t_m = (\alpha - 1)/(A\ H \exp(-E_r/RT)). \qquad [3]$$

Equation [3] shows that the existence of a peak maximum in the CH_4 rate response obtained during isothermal hydrogenation implies that there is more than one step which controls the overall hydrogenation process. If this is true, experiments at different hydrogenation temperatures, for a given CO/H_2 reaction time and temperature, should result in different t_m values. A plot of Ln (t_m) vs $1/T$ should

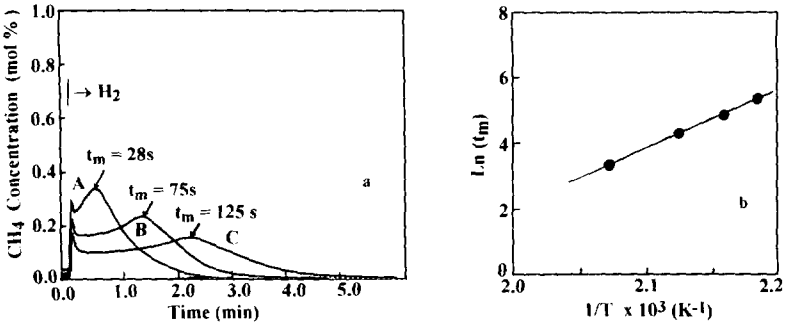

FIG. 8. (a) Transient CH_4 responses obtained according to the delivery sequence CO/H_2 (220°C, 120 s) → cool in CO/H_2 to T → H_2 (t). Curve A: T = 209°C; curve B: T = 198°C; curve C: T = 190°C. (b) Plot of Ln (t_m) vs $1/T$ for the isothermal hydrogenation experiments shown in (a).

result in a straight line according to Eq. [4]:

$$\text{Ln}\,(t_m) = \text{Ln}\,((\alpha - 1)/(AH)) + (E_r/R)(1/T). \quad [4]$$

Figure 8a presents isothermal hydrogenation results at 209°C (curve A), 198°C (curve B), and 190°C (curve C) performed according to the following experimental procedure: After reduction of the catalyst at 350°C for 2 h and a 10-min He purge, the reactor is cooled in He to 220°C and the feed is changed to CO/H_2 for 120 s. Then the reactor is cooled quickly in CO/H_2 to the hydrogenation temperature, T, at which a H_2 switch is made. The CH_4 transient responses obtained from the latter H_2 switch as a function of hydrogenation temperature are presented in Fig. 8a. There is a clear shift, towards longer times in H_2, of the time of appearance of the peak maximum of CH_4 response, t_m, as the temperature of hydrogenation decreases. Values of t_m = 28, 75, 125, and 195 s are obtained corresponding to T = 209, 198, 190, and 185°C. Using Eq. [4], a plot of Ln (t_m) vs $1/T$ is constructed, and this is shown in Fig. 8b. Note the very good fit of the data to the model, where an activation energy of E_r = 34.5 kcal/mol is obtained.

In order to justify the assumption made in the model, related to the fact that the concentration of sites for H_2 chemisorption do not change during hydrogenation, the following experiments were conducted. After reaction in CO/H_2 at 220°C for 1/2 h, the feed is changed to H_2 for time Δt, performing, therefore, hydrogenation of the adsorbed carbon species as shown in Fig. 2, followed by a 30-s Ar purge at 220°C. The reactor is then quickly cooled to 40°C in Ar flow, followed by H_2 chemisorption (1 atm H_2) and TPD according to the procedures described in Section (1d). H_2 TPD responses are shown in Fig. 9 for times in H_2, Δt, of 10 s (curve A), 60 s (curve B), and 120 s (curve C). Two H_2 peaks are seen in Fig. 9 with T_M around 110°C (first peak) and 350°C (second peak). The first peak is due to desorption of chemisorbed atomic hydrogen species on Rh, as shown by H_2 chemisorption at 40°C over a clean Rh/Al_2O_3 surface followed by a TPD conducted under the same conditions (flow rate, heating rate) as in Fig. 9. The source of the second broad H_2 peak is due to phenomena other than desorption of chemisorbed hydrogen, as is presented below. Thus, it can be seen from the first peak of Fig. 9 that after 10 s on stream in H_2 flow, following CO/H_2 reaction, the sites for H_2 chemisorption remain practically the same. For the time scale of the experiments shown in Fig. 8a, the assumption of a constant H (surface hydrogen site concentration) is, therefore, valid.

(3b) Interpretation of the second H_2 peak (T_M = 350°C) observed during TPD. During hydrogen desorption (TPD), following reaction in CO/H_2 at 220°C and H_2 chemisorption at 40°C, it is shown (Fig. 9) that after the initial narrow H_2 peak a second broad peak is recorded. Only the first peak is due to hydrogen chemisorption on the rhodium surface. The source of the second H_2 TPD peak is correlated with desorption/decomposition processes of adsorbed species as shown by the following experiments:

(a) Following CO/H_2 reaction at 220°C for 30 s or 1/2 h, the feed is changed to ^{13}CO/He for 40 s in order to exchange the adsorbed ^{12}CO with ^{13}CO. Only nonexchangeable adsorbed species such as formate, carbonate,

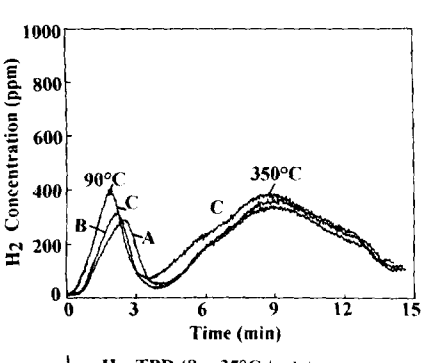

FIG. 9. H_2 TPD spectrum obtained according to the delivery sequence CO/H_2 (220°C, 1/2 h) → H_2 (Δt) → Ar (220°C, 30 s) → cool to 40°C → H_2 (40°C, 600 s) → Ar (40°C, 120 s) → TPD (β = 35°C/min). Curve A: Δt = 10 s; curve B: Δt = 60 s; curve C: Δt = 120 s.

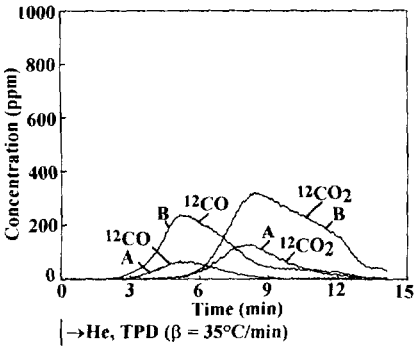

FIG. 10. CO and CO_2 responses obtained during TPD in He flow according to the delivery sequence CO/H_2 (220°C, Δt) → ^{13}CO/He (220°C, 40 s) → He (220°C, 30 s) → cool in He to 40°C → TPD (β = 35°C/min). Curve A: Δt = 30 s; curve B: Δt = 1/2 h.

and C_xH_y can give ^{12}C-containing compounds. The reactor is then purged in He at 220°C for 30 s and cooled to 40°C, followed by TPD in He. Figure 10 presents the responses of ^{12}CO and $^{12}CO_2$ (no other carbonaceous species, such as CH_4, are detected during TPD) measured by mass spectrometry during TPD in He after 30 s (curves A) and 1/2 h (curves B) on stream in CO/H_2. The corresponding H_2 response (not shown in Fig. 10) is similar to the broad peak shown in Fig. 9 and is related to the CO_2 TPD peak shown in Fig. 10. Table 3 gives the amounts of CO, CO_2, and H_2 formed during TPD in He after 30 s and 1/2 h of reaction in CO/H_2 (Fig. 10).

(b) Following CO/H_2 reaction at 220°C for 1/2 h, the feed is changed to He followed by TPD in He flow (15 K/min), while FTIR spectra in the range of 1150–2250 cm^{-1} (characteristic of all carbon–oxygen bond-containing species) (Fig. 11A), and 3000–4000 cm^{-1} (characteristic of hydroxyl groups on a surface) (Fig. 11B) are recorded. It is observed that the linear and bridged CO species have a lower desorption than hydrogenation rate

TABLE 3

Amounts of CO, CO_2, and H_2 Produced during He TPD According to the Experimental Sequence CO/H_2 (220°C, Δt) → ^{13}CO/He (40 s) → He, Cool to 40°C → He TPD

Time in CO/H_2 (Δt) (s)	CO (μmol/g)	CO_2 (μmol/g)	H_2 (μmol/g)
30	13.7	27.0	20.0
1800	56.4	95.0	145.0

(compare Figs. 6A and 11A), and these species are present during TPD even at high temperatures (spectra (e) and (f)). The amount of COOH species (bands at 1592, 1392, and 1378 cm^{-1}) decreases, while the amount of CO_3^{2-} species (band at 1460 cm^{-1}) is little affected by the TPD process in the temperature range of 220–380°C. The IR bands of the C_xH_y species decrease in intensity and disappear at around 290°C (not shown). These results indicate that the ^{12}CO and $^{12}CO_2$ responses mentioned in the previous paragraph arise from formate and $^{12}C_xH_y$ species; a small contribution of the carbonate species which need longer times of treatment at 380°C to disappear may also be considered. Therefore, the C_xH_y species gives CO and CO_2 via an oxidation process. Decomposition of the formate species may follow the route COOH → CO_2 + 1/2H_2 (33, 34). The latter remark explains the hydrogen detection simultaneously with the CO_2 production.

However, Table 3 shows that the ratio of CO_2/H (atomic hydrogen) is lower than 1 (value obtained from formate decomposition) and decreases with time on stream from 0.67 to 0.32. This means that another source of hydrogen exists on the surface. The following interpretation may be suggested. During CO/H_2 reaction, the water produced is partially adsorbed on the alumina support as hydroxyl groups characterized by IR bands at 3670 and 3570 cm^{-1}

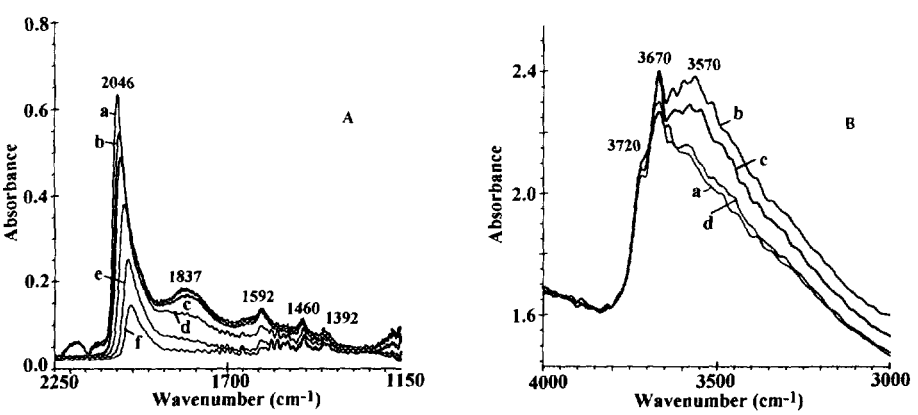

FIG. 11. (A) FTIR spectra in the range of 1150–2250 cm^{-1} recorded after CO/H_2 reaction at 220°C for 1/2 h and during He TPD, following CO/H_2 reaction. (a) after 1/2 h of CO/H_2 reaction; (b) after He purge at 220°C for 120 s; (c) T = 260°C; (d) T = 320°C; (e) T = 370°C; (f) T = 380°C. (B) FTIR spectra in the range of 3000–4000 cm^{-1} recorded during the experiment described in (A) as follows: (a) at 220°C in He flow before CO/H_2 reaction; (b) at 220°C after 1/2 h in CO/H_2; (c) at 250°C during He TPD; (d) at 370°C during He TPD.

(compare spectra (a) and (b) in Fig. 11B). During He TPD, these IR bands start to decrease (spectra (c) and (d)) and this result indicates the dehydroxylation of the alumina. The water produced from the latter process may decompose on the Rh surface to produce H_2 gas (second source of H_2) and adsorbed atomic oxygen. This oxygen may either react with the carbonaceous adsorbed species C_xH_y to produce CO and CO_2, or stay adsorbed on the Rh surface.

A comparison of the carbon mass balance obtained from the TPD experiment (Table 3), related to the adsorbed carbon species other than CO, and that obtained from the hydrogenation process shown in Fig. 4a (isothermal + TPR) (Table 2, $^{12}CH_4$ response) leads to the following remarks: For 30 s on stream, a good agreement is found, that is 0.54 of a monolayer after hydrogen titration and 0.62 after TPD. However, a difference is observed for 1/2 on stream. After hydrogen titration, 1.54 of a monolayer is obtained, while after TPD, 2.32 of a monolayer is obtained. This difference is due to the fact that carbonate and formate species, which do not fully react to CH_4 during TPR, also give CO and CO_2. These species accumulate slowly with time on stream (not detected after 30 s) and this fact explains the quantitative differences observed between the two methods of characterization.

DISCUSSION

The purpose of the present work is to *in situ* study the evolution of the adsorbed species formed during CO/H_2 reaction at 220°C on the surface of 1 wt% Rh/Al_2O_3 catalyst of 1.5-nm Rh particle size. This characterization concerns both the nature and the quantity of the adsorbed species, as well as their reactivity towards hydrogenation, exchange with gaseous ^{13}CO, and desorption in He flow.

(1) Chemical Composition of the Adsorbed Carbonaceous Species Formed during CO/H_2 Reaction at 220°C

The identification of the adsorbed carbonaceous species was mainly performed using the FTIR spectra in the ranges of 1150–2250 cm^{-1} and 2700–3100 cm^{-1} recorded during reaction at 220°C (Figs. 5A and 5B).

(1a) Infrared bands in the range of 1150–2250 cm^{-1}. The spectra shown in Fig. 5A reveal the presence of IR bands at 2046 and 1837 cm^{-1} which indicate the formation of linear and bridged adsorbed CO species on the rhodium surface, respectively (35–37). At this temperature (220°C), gem-dicarbonyl CO species are not detected. The linear CO IR band dominates, and its position and intensity stay constant with time on stream. On the other hand, a slight increase of the intensity of the IR band associated with the bridged CO species is observed during the first 10 min of reaction without any change of its position. A similar behaviour has been reported previously on the 1 wt% Ru/Al_2O_3 catalyst (38), but this concerned the IR band of the linear CO species. The authors suggested that during CO/H_2 reaction the dispersion of Ru metal may increase by converting small three-dimensional Ru particles into two-dimensional rafts, thereby exposing more metal atoms. In the present case, the effect of time on stream concerns only the bridged CO species. Taking into account the preceding remark over the Ru/Al_2O_3 catalyst (38), it is considered here that reconstruction of the Rh metal particles would have an effect only on the formation of bridged CO species, and this suggests an increase of the Rh particle size during CO/H_2 reaction. This would require a rather complex mechanism since the surface coverage of linear CO species does not change with reaction time. Another interpretation to consider is that the increase of the intensity of the bridged CO IR band may be due to the slow accumulation of other adsorbed species on the rhodium surface which interact with the bridged CO species.

The other IR bands shown in the spectra of Fig. 5A indicate that the coverages of the corresponding adsorbed species change with time in CO/H_2 reaction. The intensity of the IR bands detected at 1592, 1460, 1392, and 1378 cm^{-1} increases continuously with time on stream, even after 1 h of CO/H_2 reaction. Similar bands (position and relative intensity) have been observed on various ruthenium supported catalysts during CO/H_2 reaction, for example, over 5% Ru/Al_2O_3 (39) (1585, 1460, 1392, and 1378 cm^{-1}) and 1% Ru/Al_2O_3 (38) (1590, 1450, 1390, and 1370 cm^{-1}). The IR bands at 1592, 1392, and 1378 cm^{-1} are commonly observed on oxide catalysts for methanol synthesis, and it has been reported that, on alumina alone, these bands are formed in the presence of CO and traces of water (39). They are attributed to formate adsorbed species; 1585 cm^{-1} = ν_{as} COO, 1378 cm^{-1} = ν_SCOO, and 1392 cm^{-1} = δ CH (34, 40, 41). Some discussion is appropriate for the attribution of the 1392 cm^{-1} band to a CH bond since the intensity of the δ CH infrared bands is usually lower than that of COO bands. This remark leads to another interpretation which considers the bands at 1378 and 1392 cm^{-1} as two ν_SCOO of two formate species having the same ν_{as}COO at 1585 cm^{-1} (34, 42). According to this interpretation, the δ CH is not detected. Taking into account the difference between the ν_{as}COO and the ν_SCOO, which is larger than 200 cm^{-1}, the structure of the formate is bidentate rather than unidentate (43). Thus, the three IR bands at 1592, 1392, and 1378 cm^{-1} observed in this work are attributed to the presence of formate on the alumina support in agreement with previous work (38, 39, 44).

The 1460 cm^{-1} IR band is observed in many studies and is related to CO_2 adsorption on metal oxides. It is

attributed to ionic carbonate species, CO_3^{2-}, which is the only carbonate giving only one IR band in the region of 1700–1150 cm^{-1} (39, 45). The formation of the formate and carbonate species on the alumina support explains the fact that these species are not hydrogenated with a significant rate at 220°C as compared with the other adsorbed species present on the Rh surface (compare Figs. 5 and 6).

(1b) Infrared bands in the range of 2700–3100 cm^{-1}. The IR bands in the range of 3100–2700 cm^{-1} (bands at 2950, 2910, and 2847 cm^{-1} in Fig. 5B) are also related to carbonaceous adsorbed species. Similar bands have also been observed on various Ru catalysts (38, 39, 44, 46, 47) during CO/H_2 reaction but with the 2950 cm^{-1} band appearing as a shoulder of the 2910 cm^{-1} band and not as the most intense band, a result which is observed in the present study. On Rh/SiO_2 (48), IR bands have been observed at 2960, 2924, and 2852 cm^{-1} during CO/H_2 reaction but these bands were associated with species identical to those formed after acetaldehyde adsorption.

To interpret the three hydrocarbon bands (2950, 2910, and 2847 cm^{-1}) shown in Fig. 5B, one has to consider that formate species (detected after 10 min on stream) lead usually to two main IR bands (at around 2970 and 2882 cm^{-1}), with the intensity of the first band being lower by a factor of 3–4 than the intensity of the second band. The 2882 cm^{-1} band is attributed to the νCH bond and the 2970 cm^1 band is due to superposition or overtone of the fundamental frequencies associated with the Fermi resonance (40, 41, 49). In the present work, the three bands shown in Fig. 5B suggest that other adsorbed hydrogen-containing carbonaceous species are formed. These species are considered to be of C_xH_y form since no carbon–oxygen bond is detected in the range of 1700–1100 cm^{-1}. At 220°C, these C_xH_y species disappear faster during hydrogenation than during a desorption process in He flow (Figs. 7 and 10), in agreement with the observations of Bell and co-workers (38, 46). This remark is in favour of a species adsorbed on the metallic phase of the catalyst (38, 46). Dalla Betta and Shelef (39) observed similar IR bands, but, taking into account that these bands were not exchangeable after the switch $CO/H_2 \rightarrow CO/D_2$ was made, the authors considered that the species are on the alumina support. This observation mainly suggests that these species do not participate in the formation of CH_4 during CO/H_2 reaction, a conclusion consistent with the present isotopic results shown in Fig. 1 and Table 2.

After 320 s of hydrogenation at 220°C, the intensity of the CH bands has strongly decreased (compare spectra (a) and (c) in Fig. 7), while the IR bands of the formate (range 1700–1200 cm^{-1}) remained unaffected. Spectrum (c) in Fig. 7 does not correspond to one of the formate species, mainly because of the presence of the 2910 cm^{-1} band. This band seems to be due to a less active hydrocarbon species, C_β, which is slowly formed during CO/H_2 reaction (see Fig. 5B). It must be noted that the ratio of the intensities of the IR bands at 1592 and 2847 cm^{-1} after 320 s of hydrogenation is of the order of 10, a value which was found for a formate species formed on ZrO_2 after adsorption of CO (50). This means that the species which gives the IR band at 2910 cm^{-1} does not contribute significantly to the bands at 2847 cm^{-1}. This less active hydrocarbon species C_β may be formed either on the metallic surface (38) or on the acidic sites of the alumina support, the latter being able to strongly adsorb olefin compounds (39, 45). Assuming the same intensity for all CH bands, this species represents only a small fraction of the C_xH_y adsorbed species hydrogenated at 220°C.

The IR bands observed in the range of 3100–2700 cm^{-1} and recorded after 1 h of reaction must be interpreted as an overlap of spectra of various adsorbed species, which may be ordered according to their contribution to the spectra, as follows: (a) C_xH_y species hydrogenated at 220°C (formed on the Rh surface), (b) formate species (adsorbed on the alumina support), and (c) a less active hydrocarbon species, C_β, formed either on the Rh or the alumina support.

Some details on the structure of the hydrocarbon species may be obtained from the IR spectrum in the range of 3100–2800 cm^{-1}. Taking into account the stretching vibrational mode (asymmetrical and symmetrical) of $-CH_3-$ and $-CH_2-$ groups, previous studies (38, 39, 44, 46–48) attributed the pair of IR bands at 2960 cm^{-1} (asym) and 2840 cm^{-1} (sym) to methyl group ($-CH_3-$), and the pair of bands at 2910 cm^{-1} (asym) and 2840 cm^{-1} (sym) to methylene group ($-CH_2-$). It is the asymmetrical mode which permits us to make a distinction between the two groups. The intensity of the IR band of the asymmetrical mode is usually higher than that of symmetrical mode. Taking into account these remarks, the spectrum recorded after hydrogenation of adsorbed species at 220°C shows two main IR bands at 2910 and 2840 cm^{-1}. The infrared band at 2840 cm^{-1} is mainly due to formate species, with probably a small contribution of the symmetrical mode of the methylene group, the latter giving the IR band at 2910 cm^{-1}. Thus, the less active hydrocarbon species, C_β, seems to be a methylene species adsorbed either on the Rh surface or on the alumina support. A comparison between this spectrum and the one recorded after 1 h on stream shows that the hydrogenated species are mainly methyl groups (asym stretching mode at 2960 cm^{-1} with a symmetrical mode superimposed on the 2840 cm^{-1} bands). The groups $-CH_3-$ are probably not adsorbed directly on the Rh surface but consist of some chains with a low hydrogen content, such as $(CH_3)_n$–C-ads or $(CH_3)_{n-1}$–CH-ads (n = 1, 2, 3) species (51, 60). A structure like $CH_3–CH_2$ seems not to be possible since there are no

significant differences in the intensity of the CH_2 group (2910 cm^{-1}) before and after hydrogenation.

(2) Catalyst Surface Composition during CO/H_2 Reaction at 220°C and Related Remarks

Infrared spectroscopy permitted identification of most of the adsorbed surface intermediate species formed during CO/H_2 reaction at 220°C on the present 1 wt% Rh/Al_2O_3 catalyst. On the other hand, transient experiments (steady-state tracing, isotopic exchange, isothermal and temperature-programmed hydrogenation, and TPD), using mass spectrometer as a detector, permitted quantification of the surface composition of the catalyst during reaction. A comparison between the two sources of data leads to distinction between active and inactive (spectator) carbonaceous species not hydrogenated at the reaction temperature of 220°C.

FTIR results have shown that adsorbed CO species (linear and bridged) on the Rh surface are hydrogenated at 220°C within the first 3 min of the experiment (Fig. 6A). This means that CO adsorbed species contribute to the CH_4 response which produces peak 3 during isothermal hydrogenation at 220°C (Fig. 2). C_xH_y species, which contain $-CH_3$ groups, are also hydrogenated at 220°C during the first 3 min of the experiment (Fig. 7). These species also contribute to the formation of peak 3 shown in Fig. 2. Therefore, the appearance of CH_4 peak 3 is the result of an overlap between the rates of hydrogenation to CH_4 of CO and C_xH_y species; the appearance of an initial shoulder before the distinct maximum of peak 3 observed in Fig. 2 is also a related result. Column 3 in Table 1 gives the amount of CO and C_xH_y species contributing to peak 3 in Fig. 2. The individual contribution of each species to peak 3 is obtained using the isotopic deconvolution experiment. This experiment revealed that adsorbed CO species are exchangeable after ^{13}CO/He treatment, while the opposite is true for the C_xH_y species. Isothermal hydrogenation at 220°C, following the isotopic exchange, permitted the measurement of adsorbed CO (linear and bridged) based on the $^{13}CH_4$ response, while the measurement of C_xH_y species is based on the $^{12}CH_4$ response obtained (Fig. 4a). These results are summarized in Table 4. Note that the measurement of surface adsorbed CO is best obtained using the steady-state tracing experiment shown in Fig. 1.

The amount of C_xH_y species (Table 4, column 4) increases with time on stream during the first 10 min of reaction (in agreement with the FTIR results of Fig. 5B), while the amount of adsorbed CO stays practically constant with time on stream (Table 4, column 2). The increase of the intensity of the IR band of the bridged CO species with time on stream is related to an interaction of CO with an adsorbed species which grows with time on stream (such as the C_xH_y species) rather than to an increase of the number of Rh sites.

TABLE 4

Time Dependence of Surface Coverage of Carbon-Containing Species Formed during CO/H_2 Reaction at 220°C over 1 wt% Rh/Al_2O_3 Catalyst

Time in CO/H_2 (Δt) (s)	Monolayers			
	CO	CH_x	C_xH_y	COOH, CO_3^{2-}, C_β[a]
30	0.95	0.03	0.54	—[b]
60	—[c]	—[c]	—[c]	—[b]
120	0.95	0.02	—[c]	0.05
600	—[c]	—[c]	0.90	0.21
1800	0.93	0.03	0.96	0.49
3600	0.92	0.02	—[c]	0.84

[a] C_β is a hydrogen-containing carbon species hydrogenated to CH_4 at $T > 220$°C ($-CH_2$ species)

[b] The surface coverage is too small to be measured by mass spectrometer.

[c] Not measured.

The hydrogenation of adsorbed carbonaceous species at 220°C, following CO/H_2 reaction, reveals an initial overshoot (peak 2 in Figs. 2 and 3) which corresponds to the hydrogenation of a very active carbon-containing adsorbed species. This isothermal hydrogenation experiment does not permit an accurate measurement of the amount of this active carbon species due to an overlap with peak 3. However, the surface coverage of this active carbon species is obtained from the steady-state tracing experiment of Fig. 1 and is reported in Table 4, column 3. The latter experiment shows that the active carbon species which truly participates in the CH_4 formation during CO/H_2 reaction has a very small surface coverage independent of time on stream in CO/H_2 ($\theta = 0.015$–0.018 in the range of 30–3600 s). The very small surface coverage of this active carbon species explains why this species cannot be detected using FTIR spectroscopy. To reason about the chemical nature of this species, it is only known from this work that it does not exchange with gaseous or surface ^{13}CO. Considering what has been reported in the literature (6, 7) on a similar species obtained after CO/H_2 reaction over a 5 wt% Rh/Al_2O_3 catalyst, it may be proposed that this active carbon species is a CH_x species with x being zero.

The overshooting of peak 2 (after the switch from CO/H_2 to H_2) is due to the hydrogenation of an active CH_x species formed during CO/H_2 reaction, as previously mentioned. The sudden increase of the hydrogen surface coverage at the H_2 switch (due to some desorption of CO) is responsible for the observed larger intensity of CH_4 peak 2 as compared to that of peak 1 (after the switch from He to CO/H_2). This increase in the hydrogen coverage is

associated with the fact that during CO/H_2 reaction the number of sites for H_2 chemisorption is very small and decreases with time on stream ($\theta_H = 0.05$ after 30 s and $\theta_H = 0.02$ after 30 min; see Section 1(d)) under Results.

The three kinds of adsorbed carbonaceous species formed during CO/H_2 reaction at 220°C, which have already been described (adsorbed CO, CH_x, and C_xH_y), are hydrogenated in pure H_2 at the reaction temperature of 220°C. The other species present on the surface of Rh/Al_2O_3 catalyst are only hydrogenated at higher temperatures during a TPR process. These species were identified, using FTIR, as bidentate formate (HCOO), ionic carbonate, CO_3^{2-}, and a $-CH_2$ hydrocarbon species. The first two species are formed on the alumina support, and the third species may be formed either on the Rh surface or on the alumina support. An estimation of the amount of these three species with time on stream in CO/H_2 is obtained by TPR (Table 1). However, an accurate value may be obtained by TPD (Fig. 10, Table 3). Isothermal hydrogenation at 220°C provided the amount of C_xH_y species ($\theta = 0.96$ after 30 min on stream, Table 2). On the other hand, the total CO and CO_2 production during TPD (Fig. 10) leads to $\theta = 2.32$. This means that formate, carbonate, and the less active $-CH_2$ hydrocarbon species amount to $\theta = 1.36$. However, the CH_4 production during TPR, following CO/H_2 reaction for 30 min, gives $\theta = 0.49$. This discrepancy between the two experiments is due to the fact that, during TPR, CO and CO_2 are also formed, as has been discussed in a previous section. Table 4, column 5 gives the amount of COOH, CO_3^{2-}, and $-CH_2$ species, hydrogenated to CH_4 in the range of 260–450°C, which accumulate on the catalyst surface with reaction time. As mentioned above, this quantity must be seen as a minimum of the true quantity formed during reaction conditions. The true quantity of these species has only been measured after 30 s and 1/2 h of reaction time using TPD (Fig. 10, Table 3).

(3) Effects of Rh Particle Size on the Coverage of Intermediate Species Formed during CO/H_2 Reaction at 220°C

A comparison between the present work and that previously reported over the 5 wt% Rh/Al_2O_3 catalyst (6, 7), with a Rh particle size of 9.0 nm, provides information about possible effects of Rh particle size on the composition of the catalyst surface obtained under reaction conditions. In our previous study over the 5 wt% Rh/Al_2O_3 catalyst (6, 7), and for the same experimental conditions ($T = 220$°C, $H_2/CO = 9$, $P_{CO} = 0.1$, $X_{CO} < 1\%$), it was found that the surface coverage of CH_x species is of the same order of magnitude (3–5% of a monolayer) as that found over the present catalyst of 1.5 nm of Rh particle size. However, on the 5 wt% Rh/Al_2O_3 the coverage of the CO adsorbed species decreases with time on stream from $\theta_{CO} = 0.87$, after 120 s on stream, to 0.6, after 1 h on stream. The amount of hydrocarbon species C_xH_y formed on the Rh surface is found to increase with time on stream. For the same time on stream, the quantities of C_xH_y formed ($\theta = 1.47$) is higher over the 5 wt% Rh(9.0 nm)/Al_2O_3 than on the 1 wt% Rh (1.5 nm)/Al_2O_3 ($\theta = 0.9$) catalyst. On the other hand, the amount of carbon species hydrogenated at $T > 220$°C during TPR is found to be of the same order of magnitude, for the same time on stream. This is in agreement with the fact that in the present study it has been shown that these species are mainly formate and ionic carbonate formed on the alumina support. Recent transient FTIR results (52) have also confirmed the presence of formate and carbonate on the support of the 5 wt% Rh/Al_2O_3 catalyst.

The present results, and those previously reported over the 5 wt% Rh/Al_2O_3 catalyst (6, 7), indicate that the TOF_{CH_4} at 220°C over the latter catalyst formulation is larger by a factor of 4. Taking into account the surface composition of both catalysts under the same CO/H_2 reaction conditions, some remarks can be given. First, on both catalysts the coverage of adsorbed CO species is large ($\theta_{CO} = 0.6$–0.9) and that of CH_x low ($\theta_{CH_x} < 0.05$) during reaction conditions. These results imply that dissociation of CO largely influences the methanation reaction rate. However, this step does not control completely the reaction pathway for methane production since, during steady-state tracing (Fig. 1), the $^{13}CH_4$ response would be essentially superposed on that of ^{13}CO response, and the CH_x coverage would be immeasurably small, which is the opposite to that found (Table 4). This means that hydrogenation steps of CH_x intermediate species could influence the kinetics of methane production as well.

From the measurements of the CH_x and CO coverages on both Rh/Al_2O_3 catalysts, it is clear that neither quantity could explain the difference, by a factor of 4, in the methane turnover frequency observed between the two catalysts. Some other kinetic factors must be responsible for this behaviour. For example, considering the dissociation step of the linear CO species, vacant sites are required for the adsorption of atomic oxygen. This means that the coverage of vacant sites may affect the rate of dissociation of CO during reaction, and, therefore, the rate of CH_4 production. According to the values of the coverages of CH_x, CO, and C_xH_y adsorbed species, the coverage of vacant sites, θ_V, must be low, and a small difference in the coverage of either one of these species (C_xH_y or CH_x) over the two Rh/Al_2O_3 catalysts may strongly affect their corresponding θ_V values. The same argument could be used for the hydrogen chemisorption sites. It is easy to show that a small change (1 kcal/mol) in the activation energy of one of the elementary steps (dissociation or

hydrogenation) could also explain the difference in the turnover frequencies of methane production obtained over the two Rh particle sizes. Therefore, based on all of these remarks it becomes rather clear that it is difficult to justify the origin of the effect of particle size on the methane turnover frequency taking into account only one or two kinetic parameters from those mentioned above.

Particle size effects in the CO/H_2 reaction over group VIII metal-supported catalysts are in general considered to be small (53). It is also interesting to mention that large effects on the turnover frequency of methane production over metal-supported catalysts have been reported with respect to the chemical composition of support (54, 55). These effects have been attributed to the different rate constant, k, of the dissociation step of CO among the various Rh-supported catalysts studied (54), and also to some electronic interactions between the Rh surface and the support which are induced by the dopant used in the lattice of the metal oxide support (55).

(4) *Remarks on the Kinetics*

Some further remarks on the kinetics of CO hydrogenation, in addition to those given in the previous section, are considered here. The average rate constant k (s^{-1}) for the elementary step of hydrogenation of CH_x species can be calculated from the θ_{CH_x} values obtained via the steady-state tracing experiment of Fig. 1. A values of k ($k = TOF/\theta_{CH_x} = 1/\tau_{CH_x}$) between 0.2 and 0.3 s^{-1} is found for $T = 220°C$. Over the 5 wt% Rh(9.0 nm)/Al_2O_3 catalyst a value of k between 0.4 and 0.8 s^{-1} has been obtained at 220°C (6, 7). These values are similar to those obtained for Rh/SiO_2 ($k < 0.2$ s^{-1}, Ref. (15)), Rh/MgO ($k = 0.4$ s^{-1}, Ref. (8)), Ru/SiO_2 ($k = 0.18$ s^{-1}, Ref. (56)), Ru/TiO_2 ($k = 0.41$ s^{-1}, Ref. (56)), and Pt/TiO_2 ($k < 0.5$ s^{-1}, Ref. (57)). On the other hand, k values for Ni/Al_2O_3 (10) and Raney Ni (58) catalysts were found to be lower by about two orders of magnitude. The interpretation of the differences in the values of the rate constant k of the hydrogenation step of CH_x species to methane must be made with caution, since the dependence of the methanation turnover frequency on the hydrogen coverage is incorporated into k. Thus, before attempting to draw any conclusions about the effect of metal or support on the intrinsic k of the hydrogenation step of CH_x species, the dependence of k on the hydrogen coverage must be known.

For the Rh/Al_2O_3 (Ref. (7) and the present work), Rh/SiO_2 (15), and Rh/MgO (8), the coverage of active CH_x species is very low ($\theta_{CH_x} < 0.1$), whereas that of CO is high ($0.6 < \theta_{CO} < 0.9$). These results suggest that, for Rh supported on Al_2O_3, SiO_2, and MgO, the step which mainly controls methanation reaction is the dissociation of surface CO. However, the possibility that the low value of θ_{CH_x} may be restricted by the availability of active sites for CO dissociation cannot be excluded. On the other hand, for Ru (59), Ni (10), and Fe (11) supported on Al_2O_3, the θ_{CO} is 0.75, 0.5, and less than 0.1, respectively. In addition, the θ_{CH_x} is relatively high on Ni/Al_2O_3 (10) and Fe/Al_2O_3 (11) catalysts. For Ni and Fe supported on Al_2O_3 (10, 11), the hydrogenation step of CH_x may seem to control the rate of methane formation.

The observed decrease in the TOF of methane formation, approximately 20% after 1 h of reaction time, coincides with the increase in the surface coverage of C_xH_y hydrocarbon adsorbed species but not with any change in the θ_{CH_x} or θ_{CO} (see Table 4). It may be speculated that some of these inactive (spectator) species must decrease the coverage of empty sites θ_V, and also the number of sites for hydrogen chemisorption, therefore decreasing the methanation rate.

Figure 9 shows that, after approximately 10 s of hydrogenation at 220°C, the coverage of the hydrogen sites increases from the inital value of $\theta_H = 0.05$ to $\theta_H = 0.32$. For longer times on stream, the increase of θ_H becomes smaller ($\theta_H = 0.48$ after 120 s of hydrogenation). The recovering of hydrogen sites is related to the hydrogenation of the CO adsorbed species, the latter hydrogenated first according to the isotopic deconvolution experiment of Fig. 4, followed by the hydrogenation of C_xH_y species. The decrease of the number of sites for hydrogen chemisorption with time on stream in CO/H_2 explains the observed shift of CH_4 peak 3 maximum with time on stream (Fig. 2b) according to a previous work (32). The isotopic deconvolution experiment (Fig. 4a) indicates that only the $^{12}CH_4$ response, due to the hydrogenation of C_xH_y species, is affected by the time on stream in CO/H_2. The $^{13}CH_4$ response, due to the hydrogenation of CO, is only slightly affected. Therefore, the decrease of the number of hydrogen sites with time on stream does not affect to the same extent the CO and C_xH_y hydrogenation kinetics; this aspect will be developed further in a subsequent paper and is related to the mechanism of the hydrogenation process. Considering the kinetic model described previously (32), the shift of peak 3 maximum (t_m value) with temperature of hydrogenation (Fig. 8a) is used to evaluate kinetic parameters of the hydrogenation process of C_xH_y species. These results show that the hydrogenation of C_xH_y species proceeds with a mechanism having two or more steps, which influence the reaction rate, with the same rate constant k and an activation energy of 34 kcal/mol. In addition, the good fitting of the results to the model (Fig. 8b) suggests that indeed the hydrogen concentration stays practically constant during the isothermal hydrogenation process of the C_xH_y species. The latter result agrees with the hydrogen chemisorption measurements obtained after various times of hydrogenation (see Fig. 9).

CONCLUSIONS

The following conclusions can be drawn from the results of the present work.

(1) The rate of the CO/H_2 reaction at 220°C over 1 wt% Rh(1.5 nm)/Al_2O_3 catalyst is largely controlled by the rate of dissociation of surface CO, a conclusion similar to that drawn for the 5 wt% Rh(9.0 nm)/Al_2O_3 catalyst (6, 7).

(2) There is present on the Rh surface a large pool of surface CO and a very small pool of active carbon CH_x through which the carbon from CO passes as it forms CH_4. The same behaviour is also true over larger Rh particles (9.0 nm) supported on alumina (6, 7). However, the surface coverage of CO for the latter case largely decreases with time on stream in CO/H_2, a result which is opposite to that found in the present work.

(3) C_xH_y hydrocarbon adsorbed species (containing $-CH_2$ and $-CH_3$ groups) are formed on the Rh surface during CO/H_2 reaction at 220°C. These species largely grow with reaction time but are inactive (spectator) during methanation reaction. However, they are hydrogenated to CH_4 in pure H_2 at 220°C with an activation energy of 34 kcal/mol and they do not exchange with gaseous or adsorbed ^{13}CO.

(4) A small amount of inactive (spectator) hydrocarbon species C_β (likely of $-CH_2$ structure) is also formed on the catalyst surface. This species is hydrogenated to CH_4 in the temperature range of 260–450°C.

(5) Formate and ionic carbonate species are formed on the alumina support during CO/H_2 reaction at 220°C. These species accumulate on the Rh surface with a lower rate than the C_xH_y species do, and they do not contribute to the formation of CH_4 during CO/H_2 reaction at 220°C (spectator species).

(6) The reasons for the difference in the turnover frequency of methane formation obtained over 1.5-nm Rh particles (present work) and 9.0-nm Rh particles (6, 7) supported on Al_2O_3 cannot be ascribed to only one or two kinetic parameters which control the reaction process.

ACKNOWLEDGMENT

Support of this work was provided by the National Science Foundation, by the University of Connecticut Research Foundation, and by NATO Exchange Program 85/0669.

REFERENCES

1. Happel, J., Suzuki, I., Kokayeff, P., and Fthenakis, V., *J. Catal.* **65,** 59 (1980).
2. Happel, J., "Isotopic Assessment of Heterogeneous Catalysis." Academic Press, New York, 1986, and references therein.
3. Biloen, P., Helle, J. N., van den Berg, F. G. A., and Sachtler, W. M. H., *J. Catal.* **81,** 450 (1983).
4. Biloen, P., *J. Mol. Catal.* **21,** 17 (1983).
5. Zhang, X., and Biloen, P., *J. Catal.* **98,** 468 (1986).
6. Efstathiou, A. M., and Bennett, C. O., *J. Catal.* **120,** 118 (1989).
7. Efstathiou, A. M., and Bennett, C. O., *J. Catal.* **120,** 137 (1989).
8. Efstathiou, A. M., *J. Mol. Catal.* **67,** 229 (1991).
9. Stockwell, D. M., and Bennett, C. O., *J. Catal.* **110,** 354 (1988).
10. Stockwell, D. M., Chung, J. S., and Bennett, C. O., *J. Catal.* **112,** 135 (1988).
11. Stockwell, D. M., Bianchi, D., and Bennett, C. O., *J. Catal.* **113,** 13 (1988).
12. Winslow, P., and Bell, A. T., *J. Catal.* **94,** 385 (1985).
13. Yokomizo, G. H., and Bell, A. T., *J. Catal.* **119,** 467 (1989).
14. Krishna, K. R., and Bell, A. T., *in* "Proceedings, 10th International Congress on Catalysis, Budapest, 1992" (L. Guczi, F. Solymosi, and P. Tetenyi, Eds.), p. 180. Akadémiai Kiadó, Budapest, 1993.
15. Sidall, J. H., Miller, M. L., and Delgass, W. N., *Chem. Eng. Commun.* **83,** 261 (1989).
16. Mims, C. A., and McCandlish, L. E., *J. Phys. Chem.* **91** (4), 929 (1987).
17. Koerts, T., and van Santen, R. A., *J. Catal.* **134,** 13 (1992).
18. Nwalor, J. U., Goodwin, J. G., Jr., and Biloen, P., *J. Catal.* **117,** 121 (1989).
19. Peil, K. P., Goodwin, J. G., and Marcelin, G., *J. Catal.* **132,** 556 (1991), and references therein.
20. Efstathiou, A. M., Lacombe, S., Mirodatos, C., and Verykios, X. E., *J. Catal.*, in press.
21. Kalenik, Z., and Wolf, E. E., *Catal. Lett.* **9,** 441 (1991).
22. Delgass, W. N., Haller, G. L., Kellerman, R., and Lunsford, J. H., "Spectroscopy in Heterogeneous Catalysis," Academic Press, New York, 1979.
23. Balakos, M. W., Chuang, S. S. C., and Srinivas, G., *J. Catal.* **140,** 281 (1993).
24. Efsthatiou, A. M., Chafik, T., Bianchi, D., and Bennett, C. O., *in* "Proceedings, 10th International Congress on Catalysis, Budapest, 1992" (L. Guczi, F. Solymosi, and P. Tetenyi, Eds.), p. 1563. Akadémiai Kiadó, Budapest, 1993.
25. Tamaru, K., *in* "Catalysis: Science and Technology" (J. R. Anderson and M. Boudart, Eds.), Vol. 9. Springer-Verlag, New York, 1991.
26. Bertucco, A., and Bennett, C. O., *Appl. Catal.* **35,** 329 (1987).
27. Scholten, J. J. F., Pijpers, A. P., and Hustings, A. M. L., *Catal. Rev.—Sci. Eng.* **27** (1), 151 (1985).
28. Efstathiou, A. M., and Bennett, C. O., *Chem. Eng. Commun.* **83,** 129 (1989).
29. Bennett, C. O., *in* "Catalysis under Transient Conditions" (A. T. Bell and L. L. Hegedus, Eds.), Amer. Chem. Soc. Symposium Series, Vol. 178, p. 1. Amer. Chem. Soc., Washington, DC, 1982.
30. Chafik, T., Khalfallah, M., Bianchi, D., and Gass, J. L., submitted for publication.
31. Efstathiou, A. M., Ph. D. thesis, University of Connecticut, 1989.
32. Bianchi, D., and Gass, J. L., *J. Catal.* **123,** 298 (1990).
33. He, M. Y., and Ekerdt, J. G., *J. Catal.* **87,** 381 (1984).
34. Takafumi, S., and Iwasowa, Y., *J. Catal.* **129,** 343 (1991).
35. Buchanan, D. A., Hernandez, M. E., Solymosi, F., and White, J. M., *J. Catal.* **125,** 456 (1990).
36. Yates, J. T., Duncan, T. M., Worley, S. D., and Vaughan, R. W., *J. Chem. Phys.* **70,** 1219 (1979).
37. Worley, S. D., Rice, C. A., Mattson, G. A., Curtis, C. W., Guin, J. A., and Tarrer, A. R., *J. Chem. Phys.* **76,** 20 (1982).
38. Kellner, C. S., and Bell, A. T., *J. Catal.* **71,** 296 (1981).
39. Dalla Betta, R. A., and Shelef, M., *J. Catal.* **48,** 111 (1977).
40. Li, C., Domen, K., Maruya, K. I., and Onishi, T., *J. Catal.* **125,** 445 (1990).
41. Edwards, J. F., and Schrader, G. L., *J. Phys. Chem.* **88,** 5620 (1984).
42. Chauvin, C., Saussey, J., Lavalley, J. C., Idriss, H., Hindermann, J. P., Kiennemann, A., Chaumette, P., and Courty, P., *J. Catal.* **121,** 56 (1990).

43. Li, C., Sakata, Y., Maruya, K. I., Domen, K., and Onishi, T., *J. Chem. Soc., Faraday Trans. 1* **84,** 511 (1988).
44. King, D. L., *J. Catal.* **61,** 77 (1980).
45. Little, L. H., "IR Spectra of Adsorbed Species," p. 47. Academic Press, New York, 1966.
46. Ekerdt, J. G., and Bell, A. T., *J. Catal.* **58,** 170 (1979).
47. McQuire, M. W., and Rochester, C. H., *J. Catal.* **141,** 355 (1993).
48. Orita, H., Naito, S., and Tamaru, K., *J. Catal.* **90,** 183 (1984).
49. Kondo, J., Abbe, H., Sakata, Y., Domen, K., and Onishi, T., *J. Chem. Soc., Faraday Trans. 1* **84,** 511 (1988).
50. Bianchi, D., Chafik, T., Khalfallah, M., and Teichner, S. J., *Appl. Catal., A: General* **105,** 223 (1993).
51. Brandreth, B. J., Jackson, D., and Winstanley, D., *J. Catal.* **102,** 433 (1986), and references therein.
52. Efstathiou, A. M., Chafik, T., Bianchi, D., and Bennett, C. O., manuscript in preparation.
53. Che, M., and Bennett, C. O., *in* "Advances in Catalysis" (D. D. Eley, H. Pines, and P. B. Weisz, Eds.), Vol. 36, p. 55. Academic Press, San Diego, 1989.
54. Mori, Y., Mori, T., Miyamoto, A., Takahashi, N., Hattori, T., and Murakami, Y., *J. Phys. Chem.* **93,** 2039 (1989).
55. Ioannides, T., Verykios, X. E., Tsapatsis, U., and Economou, G., *J. Catal.* **145,** 491 (1994).
56. DePontes, M., Yokomizo, G. H., and Bell, A. T., *J. Catal.* **104,** 147 (1987).
57. Yang, C.-H., Soong, Y., and Biloen, P., *J. Catal.* **94,** 306 (1985).
58. Soong, Y., Krishna, K., and Biloen, P., *J. Catal.* **97,** 330 (1986).
59. Zhou, X., and Gulari, E., *J. Catal.* **105,** 499 (1987).
60. Trunschke, A., and Knozinger, H., *Catal. Lett.* **17,** 295 (1993).